

**Improved gauge actions on anisotropic lattices. II.  $\eta$  in the medium coupling region**

S. Sakai\*

*Faculty of Education, Yamagata University, Yamagata 990-8560, Japan*

A. Nakamura†

*RIISE, Hiroshima University, Higashi-Hiroshima 739-8521, Japan*

(Received 3 February 2004; published 18 June 2004)

For improved actions composed of plaquette and rectangular six-link loops,  $\eta$ , the ratio of renormalized to bare anisotropies, is calculated for  $\xi=2, 3, 4$ , and  $6$  in the  $\beta$  region where numerical simulations such as hadron spectroscopy are currently carried out. The  $\beta$  dependence of  $\eta$  for the renormalization-group-improved actions is quite different from those of the standard and Symanzik actions. In the Iwasaki and DBW2 (doubly blocked from Wilson action in two-coupling space) actions,  $\eta$  remains almost constant in a wide range of  $\beta$ , which is also different from the one-loop perturbative results, while in the case of the Symanzik action,  $\eta$  increases as  $\beta$  decreases, which is qualitatively similar to the perturbative result, but the slope is steeper. In the calculation of  $\eta$  close to and in the confined phase, we have applied a link integration method to suppress the fluctuation of the gauge field. Some technical details of the integration method are summarized.

DOI: 10.1103/PhysRevD.69.114504

PACS number(s): 11.15.Ha, 12.38.Gc

**I. INTRODUCTION**

Anisotropic lattices, with the temporal lattice spacing smaller than the spatial one, provide an effective method for precise Monte Carlo calculations of, for example, heavy quark systems, glueball masses, and the finite temperature properties of QCD. The properties of anisotropic lattices have been studied by several groups for a standard plaquette action [1–3].

On the other hand, improved actions have been proposed to obtain numerical results close to the continuum limit on relatively coarse lattices. They are useful and effective under the restrictions of current computer resources. Therefore it is worth studying the anisotropic properties of improved actions.

In our previous paper, we studied the properties of anisotropic lattices for a class of improved actions in weak coupling regions, mainly using the perturbative method [4]. The improved actions considered are composed of plaquette and six-link rectangular loops as

$$S \propto \sum [C_0 P(1 \times 1)_{\mu\nu} + C_1 P(1 \times 2)_{\mu\nu}], \quad (1)$$

where  $C_0$  and  $C_1$  satisfy the relation  $C_0 + 8C_1 = 1$ . The improved actions frequently used in simulations correspond to the following parameters:  $C_1 = -1/12$  (Symanzik's improved action [6]),  $C_1 = -0.331$  (Iwasaki's improved action [5]), and  $C_1 = -1.4088$  [the QCD TARO Collaboration's DBW2 (doubly blocked from Wilson action in two-coupling space) action [7]].

For these types of actions, we can formulate an anisotropic lattice in the same way as for the standard plaquette action,

$$S_g = \beta_\xi \left( \frac{1}{\xi_B} \sum_x \sum_{i>j} P_{ij} + \xi_B \sum_x \sum_{i \neq 4} P_{4i} \right), \quad (2)$$

where  $\beta_\xi = \sqrt{\beta_\sigma \beta_\tau}$ , and  $\xi_B$  is a bare anisotropic parameter that controls the anisotropy in the space and time directions. The anisotropy is defined as the ratio of the lattice spacings in the spatial ( $a_\sigma$ ) direction to that in the temporal ( $a_\tau$ ) direction,  $\xi_R = a_\sigma / a_\tau$ .

Due to the quantum correction,  $\xi_R$  is not equal to  $\xi_B$ ; therefore it is important to know their relationship before we start large-scale simulations on anisotropic lattices with improved actions.

The effect of quantum correction of anisotropy appears in the  $\eta$  defined by

$$\eta = \frac{\xi_R}{\xi_B}. \quad (3)$$

In the weak coupling region, the results of one-loop perturbative calculations have been very impressive in the sense that, as  $-C_1$  increases, a qualitative change is observed in the behavior of  $\eta$  as a function of  $\beta$  [4]. In the one-loop perturbative calculation,  $\eta$  is parametrized as

$$\eta(\xi, \beta, C_1) = 1 + \frac{N_c}{\beta} \eta_1(\xi, C_1). \quad (4)$$

The coefficient  $\eta_1$  decreases as  $-C_1$  increases. At approximately  $-C_1 \sim 0.18$ ,  $\eta_1$  reaches zero and then becomes negative. Therefore the dependence of  $\eta$  on  $\beta$  for the Iwasaki and DBW2 actions is opposite to that of the standard and Symanzik actions; for the former,  $\eta$  decreases as  $\beta$  decreases, while for the latter it increases.

A natural question is what would be the behavior of  $\eta$  in a smaller- $\beta$  region, where the perturbative calculations break down. In this work, we will calculate  $\eta$  at  $\xi_R = 2, 3, 4$ , and  $6$ , which will be denoted as  $\eta_2, \eta_3, \eta_4$ , and  $\eta_6$ , respectively,

\*Electronic address: sakai@e.yamagata-u.ac.jp

†Electronic address: nakamura@riise.hiroshima-u.ac.jp

in intermediate- $\beta$  regions where most current numerical simulations will be carried out.

In Sec. II, we discuss the regions of  $\beta$  used to evaluate  $\eta$  for the improved actions, and describe some details of the calculation: the matching of lattice potentials in the spatial and temporal directions, and a method for eliminating the self-energy contributions from  $\eta$ .

In Sec. III, our  $\eta$  results are presented. The behaviors of  $\eta$  in the intermediate- $\beta$  regions are quite different among the improved actions. For the Symanzik action,  $\eta$  increases monotonically as  $\beta$  decreases. The behavior is qualitatively similar to that of the one-loop perturbative results but the slopes are steeper. In the case of the Iwasaki action,  $\eta$  is close to unity in wide regions of  $\beta \geq 2.5$ . Particularly near  $\beta \sim 2.5$ , it is very close to unity, and therefore a detailed calibration of  $\xi_B$  is not necessary except for very precise simulations. For the DBW2 action,  $\eta$  is not close to 1, but has a weak  $\beta$  dependence, which means that rough calibrations give a reasonable estimation of  $\eta$ . It is found that the effects of self-energy terms on  $\eta$  are not large for these improved actions. This is consistent with the result of the Bielefeld group for the standard action. Section IV is devoted to discussion and conclusions.

In the calculation of  $\eta$ , measurements of large Wilson loops are required. Large Wilson loops suffer from huge fluctuations of the gauge fields, particularly in the confined phase or very close to the critical  $\beta$  of the finite temperature transition. To suppress the fluctuations, a link integration method has been proposed [8–10]. In this study, we applied the link integration method to these small- $\beta$  points. Here, it is very important to choose an adequate radius (optimal radius) of integration in the complex plane. In the Appendix, we will show the optimal radii for the Symanzik and Iwasaki actions.

## II. CALCULATION OF $\eta$ PARAMETER

### A. Region of coupling constant to be studied

In this work, we calculate  $\eta$  in the region of  $\beta$  where most numerical calculations are currently carried out. In the case of the standard action, hadron spectroscopy in the quenched approximation has been reported for  $5.7 < \beta < 6.2$  [11]. In these coupling constant regions, the light hadron masses are reproduced at up to 10% accuracy, which may be a limit of the quenched approximation. Therefore, we calculate  $\eta$  near these lattice spacings for the improved actions. In this subsection, we investigate the lattice spacings in the case of an isotropic lattice, because even though there is little corresponding information on anisotropic lattices, the difference in  $\Lambda$  ratio between isotropic and anisotropic lattices is small [4].

In order to estimate the lattice spacing for the improved actions on the isotropic lattice, we use the critical  $\beta$  of the finite temperature transition ( $\beta_{crit}$ ). For the standard action,  $\beta = 6.05$  corresponds to the finite temperature transition point for an  $N_T = 8$  lattice [12]. We estimate, then,  $\beta_{crit}$  at  $N_T = 8$  for the improved actions. For the tree-level-improved Symanzik action,  $\beta_{crit}$  values are reported for  $N_T = 3, 4, 5,$

TABLE I. Estimation of  $\beta_{crit}$  at  $N_T = 8$  for improved actions. The minimum  $\beta$  up to which we calculate  $\eta$  in this work is shown in the last column.

Action	Input $\beta_{crit}$	$\beta_{crit}(8)$ (method 1)	$\beta_{crit}(8)$ (method 2)	Minimum $\beta$
Standard	$\beta_{crit}(8) = 6.05$			
Symanzik	$\beta_{crit}(6) = 4.31$	4.57	4.56	4.5
Iwasaki	$\beta_{crit}(6) = 2.52$	2.78	2.32	2.5
DBW2	$\beta_{crit}(6) = 0.936$	1.28	—	$\sim 1.0$

and 6 [13], for the Iwasaki action, they have been calculated at  $N_T = 4$  and 6 by the Tsukuba group [14] and at  $N_T = 8$  by the Yamagata-Hiroshima Collaboration [15], and for the DBW2 action, they have been reported by the QCD-TARO Collaboration [7] for  $N_T = 3, 4,$  and 6.

$\beta_{crit}$  at  $N_T = 8$  [ $\beta_{crit}(8)$ ] is estimated using the two-loop asymptotic scaling relation for lattice spacing,

$$a(\beta) = \frac{1}{\Lambda} \left( \frac{6b_0}{\beta} \right)^{-b_1/(2b_0^2)} \exp\left( -\frac{\beta}{12b_0} \right), \quad (5)$$

where  $b_0 = 11/(4\pi)^2$  and  $b_1 = 102/(4\pi)^4$ . We apply two methods to determine  $\beta_{crit}(8)$ . In method 1, we use  $\beta_{crit}(6)$  of the same action and apply the relation

$$a[\beta_{crit}(8)] = \frac{6}{8} a[\beta_{crit}(6)]. \quad (6)$$

In method 2, we use  $\beta_{crit}(8)$  of the standard action and evaluate  $\beta_{crit}(8)$  of the improved actions using the  $\Lambda$  ratio [4,18]. The results are summarized in Table I.

In the case of the Symanzik action, the estimations of  $\beta_{crit}$  by the two methods coincide with each other. A similar result for  $\beta_{crit}(8)$  was obtained from an analysis of string tension [16,17].

For the Iwasaki action, some discrepancy is observed between the two estimations. Method 1 gives a closer result to that of Ref. [15], in which  $\beta_{crit}(8) = 2.73\text{--}2.75$ .

For the DBW2 action,  $\beta_{crit}(8)$  estimated by method 2 using the  $\Lambda$  ratio becomes negative. In this  $\beta$  region, the deviation from the two-loop asymptotic scaling relation will be quite large for this action. Therefore, for the estimation of  $\beta_{crit}(8)$ , we plot  $\beta_{crit}$  at  $N_T = 3, 4,$  and 6 and simply extrapolate it, which results in  $\beta \sim 1.1$  with large ambiguity. We will calculate  $\eta$  until  $\beta \sim 1.0$  for this action.

### B. Subtraction of self-energy contribution from lattice potential

The renormalized anisotropy  $\xi_R$  is defined by the ratio of lattice spacings in the spatial and temporal directions,  $\xi_R = a_\sigma/a_\tau$ . In the quenched approximation, the lattice potential has been used as a probe of the lattice spacing, which is defined in terms of the Wilson loop ratio,

$$V(p, r) = \log \left( \frac{W(p, r)}{W(p+1, r)} \right). \quad (7)$$

The lattice potentials in the spatial ( $V_s$ ) and temporal directions ( $V_t$ ) are defined by Wilson loops in the space-space and space-time planes, respectively. The lattice potential defined by Eq. (7) will become independent of the position  $p$ , when  $p$  becomes large.

The matching of the potentials in the spatial and temporal directions [19] has been used, for the calculation of  $\eta$ ,

$$V_s(\xi_B, p, r) = V_t(\xi_B, p, \xi_R \times r). \quad (8)$$

We fix a renormalized anisotropy  $\xi_R$ , and then search for a point of  $\xi_B$  where Eq. (8) is satisfied [2]. Using these  $\xi_B$  and  $\xi_R$  values,  $\eta$  is determined.

The lattice potential defined by Eq. (7) suffers from self-energy contributions. In this study, we assume the simplest parameterization for the lattice potential as

$$V_s(\xi_B, p, r) = V_s^0(\xi_B, p) + V_s^L(\xi_B, p, r), \quad (9)$$

where  $V_s^L$  is a lattice potential free from self-energy contributions. The temporal potential  $V_t(\xi_B, p, t)$  is treated similarly. For an anisotropic lattice,  $V_s^0(\xi_B, p)$  and  $V_t^0(\xi_B, p)$  may be different from each other due to the anisotropy.

In order to eliminate contributions from the self-energy term  $V^0$ , we define the subtracted potential as

$$\begin{aligned} V_s^{sub}(\xi_B, p, r, r_0) &= V_s(\xi_B, p, r) - V_s(\xi_B, p, r_0) \\ &= V_s^L(\xi_B, p, r) - V_s^L(\xi_B, p, r_0). \end{aligned} \quad (10)$$

$V_t^{sub}$  is defined in a similar manner.

The subtraction points  $r_0$  and  $t_0$  are chosen to satisfy the relation  $t_0 = \xi_R r_0$ , and matching of the potentials,  $V_t^L(t_0 = \xi_R r_0) = V_s^L(r_0)$ , should also be satisfied at these points; namely, at  $r_0$ , the lattice potentials should be free of lattice artifacts. This condition is satisfied if  $r_0$  is sufficiently large.

### C. An example of determination of $\eta$

As an example, we will show in detail the determination of  $\eta$  for the Iwasaki action at  $\beta=4.5$  and  $\xi_R=2$  on a  $12^3 \times 24$  lattice.

Let us start with the determination of the subtraction point  $r_0$ . In order to reduce statistical error, a small  $r_0$  is preferable. In the case of a small  $r_0$ , however, the systematic error due to lattice artifacts becomes large. On the other hand, in the case of a large  $r_0$ , the statistical error due to the fluctuations of the gauge field increases, and simulations with high statistics on larger lattices are required. Therefore,  $r_0$  should be chosen to be as small as possible, where lattice artifacts are sufficiently small. The optimal choice of  $r_0$  requires careful testing by trial and error.

First we calculate the ratio

$$R(\xi_B, p, r) = \frac{V_s(\xi_B, p, r)}{V_t(\xi_B, p, \xi_R \times r)}, \quad (11)$$

where  $V_s$  and  $V_t$  include the self-energy contributions. Our results are displayed in Fig. 1.  $R(p, r)$  seems to approach an asymptotic value with increasing  $r$ . On the other hand, at  $r$

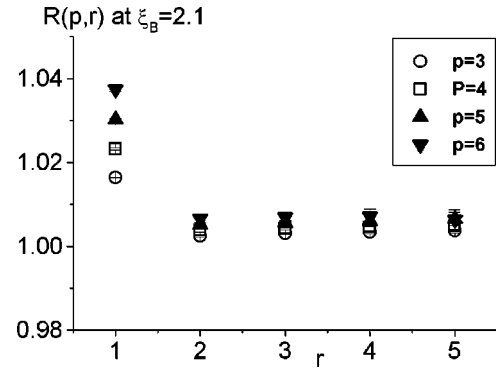


FIG. 1.  $R(p, r)$  given by Eq. (11) at  $\beta=4.5$  and  $\xi_B=2.1$  of the Iwasaki action.

$=1$ , the deviation from the asymptotic value is rather large, which may be due to lattice artifacts. Therefore, we first choose  $r_0=3$  and calculate the subtracted potentials of Eq. (10). Using the subtracted potentials, we obtain  $R$  in Eq. (11). The results for  $\xi_B=2.0, 2.1$ , and  $2.2$  are shown in Fig. 2. The  $R$  ratios are shown for each  $p$  and  $r$ . We proceed to look for the points where the ratios satisfy the relation  $R(p, r, \xi_B) = 1$ . We fit the three data points of  $R(p, r, \xi_B)$  by a second-order polynomial of  $\xi_B$  and find the solution

$$R(\xi_B, p, r) = c_0 + c_1 \xi_B + c_2 \xi_B^2 = 1. \quad (12)$$

Using the solutions  $\xi_B$  of Eq. (12),  $\eta = \xi_R / \xi_B$  is determined for each  $p$  and  $r$ , and the results are shown in Fig. 3.

In order to avoid lattice artifacts, we employ data with  $p \geq 3$  and  $r \geq 4$ . It is found that the values of  $\eta(p, r)$  are almost independent of  $p$  and  $r$  in this range.  $\eta$  at  $\beta=4.5$  and  $\xi_R=2.0$  is determined by taking their average. The error is estimated by the jackknife method; data after thermalization are grouped into ten blocks and they are used as independent data. In this way the result becomes  $\eta = 0.9755 \pm 0.0083$  when  $r_0=3$ .

The same analyses are carried out by changing  $r_0$ . The results are  $\eta = 0.9764 \pm 0.0039$  and  $\eta = 0.9741 \pm 0.010$  for  $r_0=2$  and  $4$ , respectively. The results change little among these  $r_0$  values. However, if we choose  $r_0=1$ , the result differs significantly from those of  $r_0=2, 3$ , and  $4$ . Analyses are carried out at other values of  $\beta$  and  $\xi$ . There are cases in

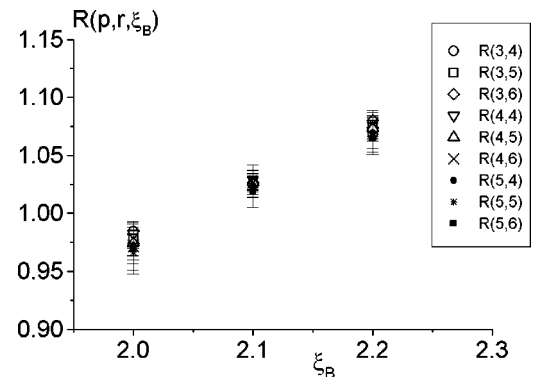
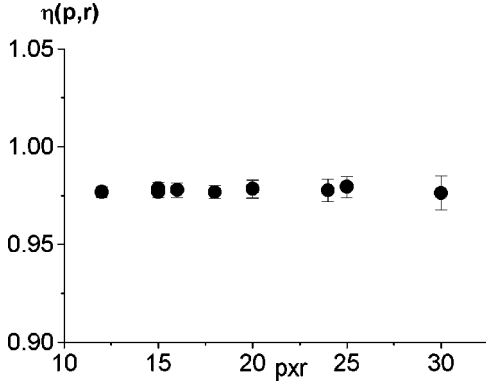


FIG. 2.  $\xi_B$  dependences of the  $R(p, r, \xi_B)$  ratios of the Iwasaki action at  $\beta=4.5$  using the subtracted potentials.

FIG. 3.  $\eta(p,r)$  of the Iwasaki action at  $\beta=4.5$  and  $\xi_R=2$ .

which a slight difference is observed between  $r_0=2$  and  $r_0=3$ , and in the case of  $r_0=4$ , the statistical error increases. Therefore in the case of the Iwasaki action we choose  $r_0=3$  for all values of  $\beta$  and  $\xi_B$  in this study.

We carried out the same studies for the Symanzik and DBW2 actions. In these cases, the subtraction point becomes  $r_0=4$ . This indicates that lattice artifacts are larger for these actions at very short distances.

### III. $\eta$ RESULTS

#### A. Simulation parameters, numerical results, and self-energy contributions

The simulations are mainly carried out for a  $12^3 \times 12 \xi_R$  lattice. For some values of  $\beta$  and  $\xi_R$ ,  $16^3 \times 16 \xi_R$  lattice simulations are also carried out in order to study the size dependence. It is found that the lattice size effect is small for the improved actions in the range of parameters studied here.

Gauge configurations are generated by the heatbath method with over-relaxation [20,21]. The typical number of Monte Carlo (MC) data for the calculation of  $R(\xi_B, p, r)$  is a few tens of thousands after a thermalization of approximately  $10^4$  MC sweeps. However, as  $\beta$  decreases and approaches the finite temperature transition point ( $\beta_{crit}$ ) or goes into a confined phase, both the number of MC data and the number of thermalization sweeps increase. For the calculation of  $\eta$  at  $\xi_R=2$  and at  $\beta=2.5$  of the Iwasaki action, we used  $1.5 \times 10^6$  data points after thermalization of  $3.5 \times 10^5$  MC sweeps.

In order to suppress the fluctuations of the gauge field in the calculations of large Wilson loops, we applied a link integration method [9,10]. It is used for calculations of lattice potentials at  $\beta=2.5$  and  $2.56$  of the Iwasaki action and at  $\beta=4.5$  of the Symanzik action. Technical details will be presented in the Appendix. Here we notice only that, in the case of the improved actions, the effect of the link integration is reduced due to the rectangular six-link loops.

Our  $\eta$  results are summarized in Tables II, III, and IV. In order to show the effects of self-energy contributions for  $\eta$ , we present the results for  $\eta$ , that are obtained without subtracting self-energy terms in the  $\eta^{no\ sub}$  column of these tables. It is found that differences between them are less than  $\sim 1\%$  for the Symanzik and Iwasaki actions. This is consis-

TABLE II.  $\eta$  for the Symanzik action at  $\xi_R=2, 3, 4$ , and  $6$ . At  $\beta=8.0$  and  $4.5$  of  $\xi_R=2$ , simulations are carried out on a  $16^3 \times 32$  lattice to study the size dependence. They are shown in the table with the symbol \*.

$\xi_R$	$\beta$	$\eta$	$\eta^{no\ sub}$
2.0	10.0	$1.0227 \pm 0.0097$	$1.0271 \pm 0.0031$
	8.0	$1.0393 \pm 0.0191$	$1.0391 \pm 0.0020$
	6.0	$1.0381 \pm 0.0097$	$1.0500 \pm 0.0029$
	4.5	$1.0980 \pm 0.0255$	$1.1011 \pm 0.0021$
	8.0*	$1.0232 \pm 0.0039$	$1.0284 \pm 0.0021$
	4.5*	$1.1095 \pm 0.0122$	$1.1040 \pm 0.0062$
3.0	10.0	$1.0341 \pm 0.0146$	$1.0426 \pm 0.0058$
	8.0	$1.0260 \pm 0.0150$	$1.0361 \pm 0.0042$
	6.0	$1.0520 \pm 0.0200$	$1.0667 \pm 0.0015$
	4.5	$1.1482 \pm 0.0317$	$1.1331 \pm 0.0064$
4.0	8.0	$1.0330 \pm 0.0180$	$1.0389 \pm 0.0042$
	6.0	$1.0876 \pm 0.0294$	$1.0786 \pm 0.0058$
	4.5	$1.1408 \pm 0.0336$	$1.1572 \pm 0.0058$
6.0	8.0	$1.0547 \pm 0.0403$	$1.0596 \pm 0.0088$
	6.0	$1.1355 \pm 0.0482$	$1.1088 \pm 0.0081$
	4.5	$1.1542 \pm 0.0587$	$1.1660 \pm 0.0170$

tent with the result for the standard action obtained by the Bielefeld group [3]. For the DBW2 action, the differences increase. They amount to approximately 5% but are still not large. Therefore, except for the case of simulations with a few percent accuracy, it is safe to use  $\eta^{no\ sub}$ , as reported at the XVIth and XVIIth International Symposium on Lattice Field Theory at Colorado and Pisa, respectively [22,23].

#### B. Symanzik action

The  $\eta$  results for Symanzik action are shown in Fig. 4.  $\eta$  at  $\xi_R=2, 3, 4$ , and  $6$  is denoted as  $\eta_2, \eta_3, \eta_4$ , and  $\eta_6$ , respectively. The qualitative behavior of  $\eta$  as function of  $\beta$  is the same in perturbative and numerical results; the slope of  $\eta$ , however, is steeper in the numerical results.

In this case, the tadpole-improved one-loop perturbation calculation (boosted perturbation) [24,25] reduces the discrepancy a little. It is expressed by replacing  $\beta$  in Eq. (4) with  $\tilde{\beta} = \beta \sqrt{W_s(1,1)W_t(1,1)}$ ; thus

$$\eta(\xi, \beta) = 1 + \frac{N_c}{\beta} \frac{\eta_1(\xi)}{\sqrt{W_s(1,1)W_t(1,1)}}. \quad (13)$$

In this formula, since  $W_s(1,1)$  and  $W_t(1,1)$  decrease as  $\beta$  decreases, the  $\beta$  dependence of  $\eta$  is more enhanced. The fit of the numerical data by Eq. (13) is shown in Fig. 5. In this figure, we also compare our results with those of the standard plaquette action [2]. In order to compare  $\eta$  at the same lattice spacing, we have shifted  $\beta$  for the standard action to that for the Symanzik action using the asymptotic scaling relation Eq. (5) and the  $\Lambda$  ratio.

TABLE III.  $\eta$  for the Iwasaki action at  $\xi_R=2, 3, 4$ , and 6. The data at  $\beta=3.5$  of  $\xi_R=2$  with an asterisk are calculated on a  $16^3 \times 32$  lattice to study the size dependence.

$\xi_R$	$\beta$	$\eta$	$\eta^{no\ sub}$
2.0	10.0	$0.9811 \pm 0.0030$	$0.9742 \pm 0.0033$
	6.0	$0.9831 \pm 0.0037$	$0.9784 \pm 0.0032$
	4.5	$0.9755 \pm 0.0083$	$0.9776 \pm 0.0044$
	4.0	$0.9806 \pm 0.0074$	$0.9782 \pm 0.0039$
	3.5	$0.9761 \pm 0.0105$	$0.9767 \pm 0.0049$
	3.05	$0.9911 \pm 0.0182$	$0.9881 \pm 0.0060$
	2.5	$0.9998 \pm 0.0145$	$0.9837 \pm 0.0074$
	3.5*	$0.9803 \pm 0.0070$	$0.9802 \pm 0.0036$
3.0	10.0	$0.9714 \pm 0.0054$	$0.9647 \pm 0.0036$
	6.0	$0.9669 \pm 0.0041$	$0.9554 \pm 0.0026$
	4.0	$0.9700 \pm 0.0118$	$0.9645 \pm 0.0063$
	3.5	$0.9715 \pm 0.0160$	$0.9708 \pm 0.0031$
	3.05	$0.9725 \pm 0.0120$	$0.9776 \pm 0.0037$
	2.56	$1.0067 \pm 0.0138$	$1.0011 \pm 0.0071$
4.0	6.0	$0.9640 \pm 0.0048$	$0.9563 \pm 0.0024$
	4.0	$0.9625 \pm 0.0105$	$0.9583 \pm 0.0039$
	3.0	$0.9851 \pm 0.0118$	$0.9852 \pm 0.0054$
	2.56	$1.0046 \pm 0.0102$	$1.0042 \pm 0.0040$
	6.0	$0.9373 \pm 0.0092$	$0.9340 \pm 0.0036$
6.0	4.0	$0.9558 \pm 0.0055$	$0.9500 \pm 0.0032$
	3.0	$0.9796 \pm 0.0109$	$0.9805 \pm 0.0087$

TABLE IV.  $\eta$  for the DBW2 action at  $\xi_R=2, 3, 4$ , and 6.

$\xi_R$	$\beta$	$\eta$	$\eta^{no\ sub}$
2.0	2.5	$0.9084 \pm 0.0090$	$0.8626 \pm 0.0025$
	1.6	$0.9011 \pm 0.0082$	$0.8616 \pm 0.0018$
	1.4	$0.8917 \pm 0.0122$	$0.8623 \pm 0.0024$
	1.2	$0.8882 \pm 0.0115$	$0.8673 \pm 0.0032$
	1.1	$0.8868 \pm 0.0144$	$0.8753 \pm 0.0030$
	1.0	$0.8781 \pm 0.01069$	$0.8817 \pm 0.0092$
3.0	1.4	$0.8283 \pm 0.0189$	$0.8082 \pm 0.0046$
	1.2	$0.8157 \pm 0.0252$	$0.8070 \pm 0.0055$
	1.1	$0.8122 \pm 0.0230$	$0.8210 \pm 0.0076$
	1.0	$0.8123 \pm 0.0235$	$0.8262 \pm 0.0101$
4.0	2.0	$0.8277 \pm 0.0202$	$0.7888 \pm 0.0087$
	1.4	$0.8068 \pm 0.0306$	$0.7789 \pm 0.0100$
	1.2	$0.7787 \pm 0.0319$	$0.7866 \pm 0.01.9$
	1.0	$0.7842 \pm 0.0172$	$0.7894 \pm 0.0140$
6.0	2.0	$0.7311 \pm 0.0183$	$0.7229 \pm 0.0103$
	1.4	$0.7326 \pm 0.0170$	$0.7349 \pm 0.0066$

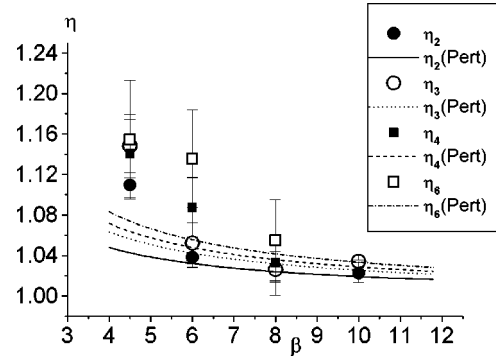


FIG. 4.  $\eta$  for the Symanzik action. Perturbative results [ $\eta(\text{pert})$ ] from Ref. [4] are shown to compare with the numerical results.

The  $\eta$  behaviors for these two actions are qualitatively the same, although the slope is gentler for the Symanzik action.

### C. Iwasaki action

The results for  $\eta$  for the Iwasaki action are shown in Fig. 6. For  $\xi_R=2, 3, 4$ , and 6,  $\eta$  remains close to unity in a wide range of  $\beta$  for  $\beta \geq 2.5$ . The deviation from unity is more enhanced for larger  $\xi_R$ , but within approximately 6%. Therefore, unless a precision simulation of a few percent accuracy is required, detailed calibration of  $\xi_B$  is not necessary. In particular,  $\eta$  is very close to unity at approximately  $\beta \sim 2.5$ , where most simulations take place. This is a good feature for the simulations, because detailed calibration is not necessary until a very precise simulation is carried out.

$\eta$  should have a dip between  $\beta \sim 2.5$  and  $\infty$ , because at approximately  $\beta \sim 2.5$  it is close to unity, and decreases as  $\beta$  increases and then approaches unity again as  $\beta$  approaches  $\infty$ . In Table III, we observe shallow dips at approximately  $\beta \sim 4.5$  and  $\beta \sim 6.0$ , for  $\eta_2$  and  $\eta_3$ , respectively. It seems that the position of the dip moves to larger  $\beta$  as  $\xi_R$  increases.

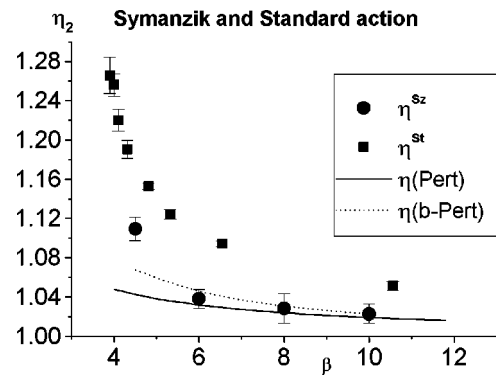


FIG. 5.  $\eta$  for the Symanzik ( $\eta^{Sz}$ ) and standard ( $\eta^{stand}$ ) actions at  $\xi_R=2$ . For the standard action, we show the results obtained by Klassen [2]. The  $\beta$  of the standard action is shifted using Eq. (5) and the  $\Lambda$  ratio, in order to compare the  $\eta$  parameters at the same lattice spacing  $a$ . The perturbative results, naive [ $\eta(\text{pert})$ ] and boosted [ $\eta(b\text{-pert})$ ] of Eq. (13), are also shown to compare with the numerical results.

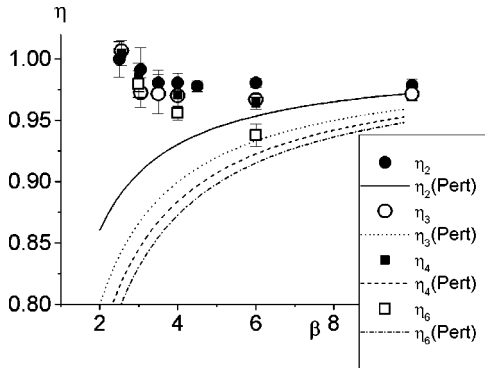


FIG. 6.  $\eta$  for the Iwasaki action. Perturbative results [ $\eta(\text{pert})$ ] from Ref. [4] are shown to compare with the numerical results.

For the Iwasaki action, the one-loop perturbative calculation predicts a monotonic decrease in  $\eta$  as  $\beta$  decreases [4]. The numerical results are qualitatively different from those of the one-loop perturbative calculation, as shown in Fig. 6.

In the continuum limit,  $\eta$  should approach unity; therefore, as far as  $\eta$  is concerned, this action is close to the continuum limit.

#### D. DBW2 action

In Fig. 7,  $\eta$  values for the DBW2 action are displayed. As  $\xi_R$  increases  $\eta$  decreases. The deviation of  $\eta$  from unity is not small, and its  $\beta$  dependence is very weak. This is again a good property for numerical simulation. Rough calibrations of  $\eta$  at a few  $\beta$  points are sufficient to obtain a reasonable estimation of  $\xi_B$ . As in the case of the Iwasaki action, the numerical results are qualitatively different from those of the one-loop perturbative calculations [4], which are also shown in Fig. 7.

### IV. DISCUSSION AND CONCLUSIONS

In this work, we studied the global structure of  $\eta$  as a function of  $\beta$ ,  $\xi_R$ , and  $C_1$  for the class of gauge actions given in Eq. (1). The overall effects of the improved actions on  $\eta$  are summarized as follows. The plaquette term in the action makes  $\eta$  increase monotonically as  $\beta$  decreases, while

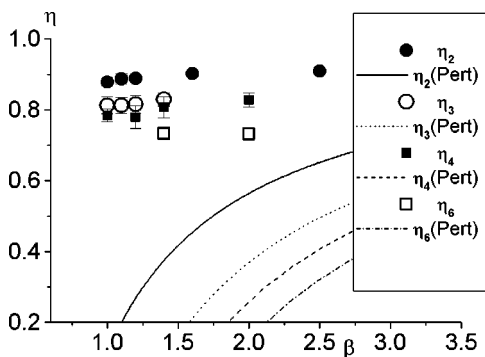


FIG. 7.  $\eta$  for the DBW2 action. Perturbative results [ $\eta(\text{pert})$ ] from Ref. [4] are shown to compare with the numerical result.

the rectangular term with  $C_1 < 0$  makes  $\eta$  decrease.

At  $C_1 = -1/12$ , the effects of rectangular loops are not so large, and the slope of  $\eta$  is smaller than that of the standard action. As a result, at the same lattice spacing, the effects of the quantum correction are reduced in the Symanzik action. In the Symanzik and standard actions, the  $\beta$  dependences of  $\eta$  are qualitatively the same between the perturbative and numerical results, but the slopes are steeper for the numerical results.

At  $C_1 = -0.331$ , the effects on  $\eta$  from the plaquette and rectangular loops are almost in balance in a wide range of  $\beta$ , for  $2.5 \leq \beta$ . However, the detailed contributions depend on  $\beta$  and  $\xi_R$ .  $\eta$  at  $\beta \sim 2.5$  is very close to 1, and decreases as  $\beta$  increases and should again approach unity at a large  $\beta$ . Therefore each  $\eta$  should have a dip in the range  $2.5 < \beta < \infty$ ; they are around  $\beta \sim 4.5$  and  $\beta \sim 6.0$  for  $\eta_2$  and  $\eta_3$ , respectively. As a consequence,  $\eta$  remains close to unity in the range  $2.5 < \beta$ . These behaviors are qualitatively different from the results of the one-loop perturbative calculation.

At  $C_1 = -1.4088$ , the contribution from the rectangular loop becomes stronger than that of the plaquette loop, and then  $\eta$  values become less than 1. They are, however, almost independent of  $\beta$  in the range  $1.0 \leq \beta \leq 2.5$ . This behavior is qualitatively different from the perturbative result.

In the continuum limit,  $\eta$  parameters should approach unity. Then the Iwasaki action is close to the continuum limit in the region  $2.5 \leq \beta$ . Particularly at approximately  $\beta \sim 2.5$ , the  $\eta$  values are close to unity. This means that calibrations of  $\xi_B$  are not necessary until a high-precision simulation is carried out.

In the case of the DBW2 action, the  $\eta$  values are not close to 1. Then, as far as  $\eta$  is concerned, it is not close to the continuum limit in this  $\beta$  region. However,  $\eta$  is almost independent of  $\beta$ . This is good for the simulation of physical quantities on anisotropic lattices, because calibrations of  $\xi_B$  at a few  $\beta$  points are sufficient for this action.

For the Symanzik action, the deviation of  $\eta$  parameter from unity is remedied compared with standard action, and yet the  $\beta$  dependence of  $\eta$  is not sufficiently weak. It becomes  $\sim 10\%$  at  $\beta \sim 5.0$ . Therefore some detailed calibrations are necessary.

For the  $\beta$  and  $\xi_R$  ranges that we have studied, the differences between  $\eta$  and  $\eta^{no\ sub}$  are small for all the improved actions. For the Symanzik and Iwasaki actions, the differences are within  $\sim 1\%$ , and for the DBW2 action, they are within  $\sim 5\%$ . Therefore it is safe to use  $\eta^{no\ sub}$  except for the case of very precise simulation. This is good news, because the calculation of  $\eta$  requires much more CPU time.

For the Symanzik action, the tadpole-improved one-loop perturbation calculation (boosted perturbation) [24,25] given by Eq. (13) improves the agreement between the simulation and perturbative results, but for the Iwasaki and DBW2 actions it makes the discrepancies larger.

Our results provide fundamental data for large-scale simulations on an anisotropic lattice using improved actions. Further results on  $\eta$  for larger  $\xi_R$  and smaller  $\beta$  will be reported when they become necessary because the calculation of  $\eta$  at smaller  $\beta$  and larger  $\xi_R$  requires much more CPU time.

## ACKNOWLEDGMENTS

This work has been carried out using the SX-5 at RCNP, Osaka University and the VX-4 at Yamagata University. We are grateful to the members of RCNP for their kind support.

## APPENDIX: OPTIMAL RADIUS OF INTEGRATION FOR IWASAKI AND SYMANZIK ACTIONS

If  $R$  is an external source field for the link variable  $U$ , integration of the link variable  $U$  is given by

$$\langle U \rangle = \frac{1}{Z} \frac{dZ(R)}{dR^\dagger} = \frac{\int D[U] U \exp[\text{Tr}(RU^\dagger + UR^\dagger)]}{\int D[U] \exp[\text{Tr}(RU^\dagger + UR^\dagger)]}, \quad (\text{A1})$$

where  $Z(R)$  is expressed by the modified Bessel function  $I_1$  [9,10],

$$Z(R) = \oint \frac{dx}{2\pi i} e^{xQ} \frac{1}{z} I_1(2z), \quad (\text{A2})$$

and

$$z = \left( \frac{P(x)}{x} \right)^{1/2},$$

$$Q = 2 \text{Re}[\det(R)],$$

$$P(x) = 1 + x \text{Tr}(RR^\dagger) + \frac{1}{2} x^2 [\text{Tr}(RR^\dagger)]^2 - \text{Tr}[(RR^\dagger)^2] + x^3 \det(RR^\dagger). \quad (\text{A3})$$

Similarly,  $dZ(R)/dR^\dagger$  is written using the modified Bessel function  $I_1$  and  $I_2$  [9,10],

$$\begin{aligned} \frac{dZ(R)}{dR^\dagger} &= \oint \frac{dx}{2\pi i} x e^{xQ} \frac{1}{z} I_1(2z) \frac{\partial Q}{\partial R^\dagger} \\ &+ \oint \frac{dx}{2\pi i} \frac{e^{xQ}}{P(x)} I_2(2z) \frac{\partial P(x)}{\partial R^\dagger}. \end{aligned} \quad (\text{A4})$$

The path of the integration is a closed circle on the complex plane  $x$ . In principle it is arbitrary, but numerical integration requires an adequate radius. In the case of the standard action, the adequate radius has been studied [26].

The arguments of the modified Bessel functions become rather large and we apply an asymptotic expansion for numerical integration. In this article we use the Simpson method for numerical integration and search for the region of  $r$  where  $\langle U \rangle$  is stable under a change of  $r$ , at a given number of divisions  $N$ .

An example of the  $r$  dependence of  $\langle U \rangle$  is shown in Fig. 8. It is found that when  $N=100$  some spurious plateaus appear and then disappear when  $N=400$ . However, there is a region of  $r$  where  $\langle U \rangle$  is stable under changes of  $N$ , which is the optimal region of integration for  $N=100$ . The optimal region increases a little when  $N=400$ . In this article we

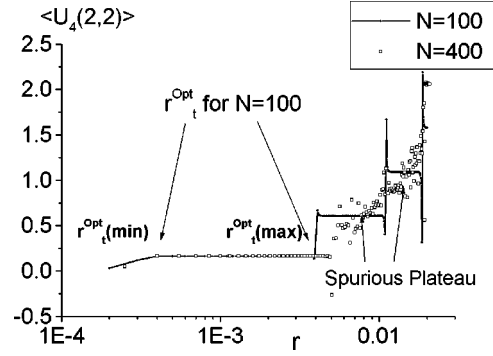


FIG. 8. Radius dependence of  $\langle U_4(2,2) \rangle$  for the Iwasaki action at  $\beta=3.05$  and  $\xi_B=2.0$ . An integrated link is located at the center of the lattice, directed in the fourth (temporal) direction, on a fully thermalized configuration.

choose  $N=100$  and proceed to determine the optimal region of  $r$  ( $r^{\text{opt}}$ ) for various combinations of  $\beta$  and  $\xi_B$ .

These plateaus shown in Fig. 8 are observed when Taylor expansions of the modified Bessel functions are applied. Then they are due to the difficulty in numerical integrations given by Eqs. (A2) and (A4). Therefore it is important to find the optimal  $r$  region.

For many sets of  $\beta$  and  $\xi_B$ , we have obtained the minimum of  $r^{\text{opt}}$  [ $r^{\text{opt}}(\text{min})$ ] and its maximum [ $r^{\text{opt}}(\text{max})$ ] for spacelike and timelike links separately. When  $\xi > 1.0$ , the  $r^{\text{opt}}$  of timelike links ( $r_t^{\text{opt}}$ ) is smaller than that of spacelike links ( $r_s^{\text{opt}}$ ). Examples of the differences are shown in Fig. 9. It seems that the difference becomes larger as  $\beta$  and  $\xi_B$  increase.

We proceed to a parametrization of  $r^{\text{opt}}(\beta, \xi)$ . The  $\beta$  and  $\xi$  ranges are  $2.0 \leq \beta \leq 6.0$ ,  $1.8 \leq \xi_B \leq 6.5$  for the Iwasaki action and  $4.5 \leq \beta \leq 8.0$ ,  $1.7 \leq \xi_B \leq 5.8$  for the Symanzik action. The  $r_s^{\text{opt}}(\text{min})$  and  $r_s^{\text{opt}}(\text{max})$  are shown in Fig. 10. They decrease with  $\beta$  and  $\xi$  and seem to be parametrized as

$$r^{\text{opt}} = a \exp(-b\beta - c\xi_B). \quad (\text{A5})$$

Then we define  $r^{\text{opt}}(\text{mid})$

$$\log[r^{\text{opt}}(\text{mid})] = \{\log[r^{\text{opt}}(\text{min})] + \log[r^{\text{opt}}(\text{max})]\}/2 \quad (\text{A6})$$

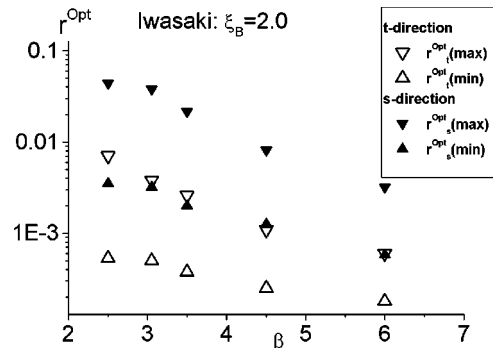


FIG. 9. Examples of the difference between  $r_s^{\text{opt}}$  and  $r_t^{\text{opt}}$  for the Iwasaki action at  $\xi_B=2.0$ .

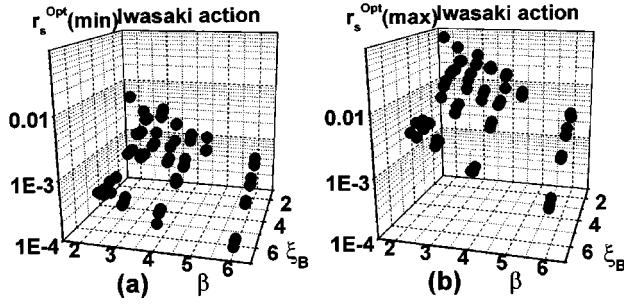


FIG. 10. A compilation of (a)  $r_s^{opt}(\min)$  and (b)  $r_s^{opt}(\max)$  of the Iwasaki action in the range  $2.0 \leq \beta \leq 6.0$  and  $2.0 \leq \xi_B \leq 6.0$ .

and then fit them using Eq. (A5). The coefficients  $a$ ,  $b$ , and  $c$  are determined by least squares. The results for the Symanzik and Iwasaki actions are summarized in Table V.

We have checked that  $r^{opt}(\text{mid})$  with the parameters given in Table V is located between  $r^{opt}(\max)$  and  $r^{opt}(\min)$ ; namely, it stays within the optimal radius of integration throughout the data points.

The  $r^{opt}$  region depends on the background field of each link variable. Thus it suffers from fluctuations of gauge field of links and configurations. The results shown in Fig. 10 are obtained for a link at the center of a configuration in the

TABLE V. The fit of  $r^{opt}(\text{mid})$  by Eq. (A5). 61 and 29 data points are used to determine the coefficients  $a$ ,  $b$ ,  $c$  for the Iwasaki and Symanzik actions, respectively.

Action		$a$	$b$	$c$
Symanzik (26 data)	$r_s^{opt}(\text{mid})$	0.5563	0.5479	0.5336
	$r_t^{opt}(\text{mid})$	0.06244	0.4213	0.6568
Iwasaki (61 data)	$r_s^{opt}(\text{mid})$	0.08663	0.5507	0.4315
	$r_t^{opt}(\text{mid})$	0.01682	0.5139	0.5261

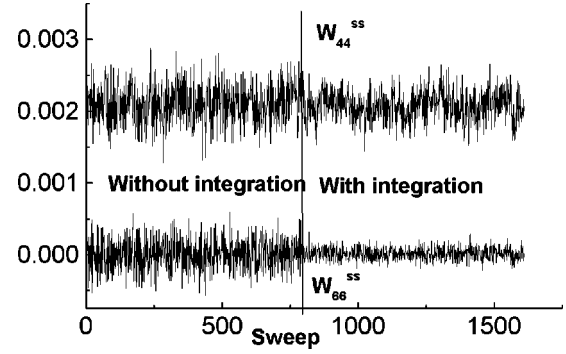


FIG. 11. Example of the suppression of the fluctuation of Wilson loops for the Iwasaki action at  $\beta=2.5$  and  $\xi_B=2.0$ .

space and time directions that is fully thermalized. However, the fluctuation of the  $r^{opt}$  region is not large, compared with the width of  $r^{opt}$ .  $r^{opt}(\text{mid})$ , parametrized by Eq. (A5) with the coefficients given in Table V, was in the optimal region of  $r$  for all link variables and configurations.

Let us proceed to discuss the effects of the link integration method. In the case of the improved actions, the number of links  $U$  which are simultaneously integrated in a Wilson loop becomes much smaller than in the case of a standard action, because in the case of the improved action the background fields  $R$  of Eq. (A1) extend over a wider range due to the six-link rectangular loops in the action. Therefore the effect of the link integration method is reduced for the improved actions and it is not effective for the calculation of smaller Wilson loops.

An example of the suppression of the fluctuation is shown in Fig. 11. The suppression is marked for  $W(6,6)$  but not for  $W(4,4)$ . Similar properties are observed for the Symanzik action of  $W(8,8)$  and  $W(4,4)$  at  $\beta=4.5$  and  $\xi_B=1.9$ . The link integration method requires much CPU time. Therefore, when the fluctuation of the gauge field is not sufficiently large, there are cases where a result is obtained with less CPU time if the link integration method is not applied. Those cases correspond to  $\beta$  values far above  $\beta_{crit}$ . However, in the cases of a confined phase or very close to the transition point, the link integration method is indispensable.

[1] F. Karsch, Nucl. Phys. **B205** [FS5], 285 (1982).  
[2] T.R. Klassen, Nucl. Phys. **B533**, 557 (1998).  
[3] J. Engels, F. Karsch, and T. Scheideler, Nucl. Phys. **B564**, 303 (2000).  
[4] S. Sakai, T. Saito, and A. Nakamura, Nucl. Phys. **B584**, 528 (2000).  
[5] Y. Iwasaki, Nucl. Phys. **B258**, 141 (1985); University of Tsukuba Report No. UTHEP-118, 1983.  
[6] K. Symanzik, Nucl. Phys. **B226**, 187 (1983); M. Lüscher and P. Weisz, Phys. Lett. **158B**, 250 (1985).  
[7] QCD-TARO Collaboration, Ph. de Forcrand *et al.*, Nucl. Phys. **B577**, 263 (2000).  
[8] G. Parisi, R. Petronzio, and F. Rapuano, Phys. Lett. **128B**, 418 (1983); Nucl. Phys. **B205** [FS5], 337 (1982).  
[9] R. Brower, P. Rossi, and C.I. Tan, Nucl. Phys. **B190** [FS3], 699 (1981).

[10] Ph. de Forcrand and C. Roiesnel, Phys. Lett. **151B**, 77 (1985).  
[11] T. Yoshie, Nucl. Phys. B (Proc. Suppl.) **63**, 3 (1998).  
[12] QCD-TARO Collaboration, Ph. de Forcrand *et al.* (private communication).  
[13] G. Cella, G. Curci, A. Vicere, and B. Vigna, Phys. Lett. B **333**, 457 (1994).  
[14] Y. Iwasaki, K. Kanaya, T. Kanenko, and T. Yoshie, Nucl. Phys. B (Proc. Suppl.) **53**, 429 (1997).  
[15] A. Nakamura, T. Saito, and S. Sakai, Nucl. Phys. B (Proc. Suppl.) **63**, 424 (1998).  
[16] A. Peikert, Ph.D. thesis, Bielefeld, 2000, Appendix C.  
[17] B. Beinlich, F. Karsch, E. Laermann, and A. Peikert, Eur. Phys. J. C **6**, 133 (1999).  
[18] Y. Iwasaki and S. Sakai, Nucl. Phys. **B248**, 441 (1984).

- [19] G. Burgers, F. Karsch, A. Nakamura, and I.O. Stamatescu, Nucl. Phys. **B304**, 587 (1988).
- [20] F.R. Brown and T.J. Woch, Phys. Rev. Lett. **58**, 2394 (1987).
- [21] M. Creutz, Phys. Rev. D **36**, 515 (1987).
- [22] S. Sakai, A. Nakamura, and T. Saito, Nucl. Phys. B (Proc. Suppl.) **73**, 417 (1999).
- [23] S. Sakai, A. Nakamura, and T. Saito, Nucl. Phys. B (Proc. Suppl.) **83-84**, 399 (2000).
- [24] G. Martinelli, G. Parisi, and R. Petronzio, Phys. Lett. **100B**, 435 (1981).
- [25] G.P. Lepage and P.B. Mackenzie, Phys. Rev. D **48**, 2250 (1993).
- [26] T. Scheideler, Ph.D. thesis, Bielefeld, 1997.